Effects of carrier concentration on the dielectric function of ZnO:Ga and In_2O_3:Sn studied by spectroscopic ellipsometry: Analysis of free-carrier and band-edge absorption

Hiroyuki Fujiwara* and Michio Kondo
Research Center for Photovoltaics, National Institute of Advanced Industrial Science and Technology (AIST), Central 2, Umezono 1-1-1, Tsukuba, Ibaraki 305-8568, Japan
(Received 28 September 2004; published 15 February 2005)

We have determined the dielectric functions of ZnO:Ga and In_2O_3:Sn with different carrier concentrations by spectroscopic ellipsometry. The dielectric functions have been obtained from ellipsometry analyses using the Drude and Tauc-Lorentz models. With increasing Hall carrier concentration N_{Hall} in a range from 10^{19} to 10^{21} cm^{-3}, the dielectric functions of ZnO:Ga and In_2O_3:Sn show drastic changes due to increases in (i) free-carrier absorption in a low-energy region and (ii) the Burstein-Moss shift in a high-energy region. The analyses of the dielectric functions revealed reductions in high-frequency dielectric constant ε_∞ and increases in plasma energy E_p as N_{Hall} in the films increases. From a set of the parameters (N_{Hall}, ε_∞, E_p) determined experimentally, effective mass m^* of ZnO:Ga and In_2O_3:Sn is extracted. In contrast to previous studies, we found linear increases in m^* with increasing N_{Hall}. When the variations of m^* with carrier concentration are taken into account, carrier concentrations determined optically from spectroscopic ellipsometry show remarkable agreement with those estimated by Hall measurements. Nevertheless, the electron mobility obtained from spectroscopic ellipsometry and Hall measurements indicates rather poor agreement. We attributed this to the presence of grain boundaries in the films. In this article, we discuss various effects of carrier concentration on the optical properties of transparent conductive oxides.

DOI: 10.1103/PhysRevB.71.075109 PACS number(s): 77.22.Ch, 78.20.Ci, 78.20.Jq

I. INTRODUCTION

Transparent conductive oxides (TCO's), such as doped ZnO and In_2O_3:Sn, have become increasingly important by recent developments of optoelectronic devices including solar cells.[1–3] Although a considerable number of studies have been made on the TCO's,[4–41] there still has been a fundamental requirement for a clear understanding of physical backgrounds that determine the optical constants of the TCO's. Such an understanding is of significant importance for the interpretation and prediction of optical constants in various TCO's.

Nevertheless, the determination of optical constants has been rather difficult in the TCO's, mainly owing to three physical factors including (i) a strong variation of free-carrier absorption with carrier concentration,[6,7,11] (ii) a shift of band-edge absorption with carrier concentration,[6–8] and (iii) a large dependence of carrier concentration on thin-film thickness.[9–14] In particular, both doped ZnO and In_2O_3:Sn incorporated into optoelectronic devices generally have high carrier concentrations of $\sim 10^{20}$ cm^{-3}. At these carrier concentrations, however, light absorption by free carriers alters the optical constants significantly in a range extending from the near-infrared to visible region.[6,7,11]

In addition, when the carrier concentration in the TCO's exceeds the Mott critical density [10^{18}–10^{19} cm^{-3} in ZnO (Ref. 15) and In_2O_3:Sn (Ref. 6)], a semiconductor-to-metal transition occurs and conduction band filling with free electrons shifts the onset of band-edge absorption in the ultraviolet region (Burstein-Moss shift).[6–8] Thus, by variations of the free-carrier absorption and Burstein-Moss shift, the overall optical constants change drastically in a quite wide range from the near-infrared to ultraviolet region.[6,7]

The large dependence of carrier concentration on film thickness further complicates the characterization of the TCO's. This variation is caused primarily by improvements of polycrystalline grain structures with thin-film thickness.[9,10,13] Deposition methods and the type of doping atom appear to have weak effects on the variation. In fact, all polycrystalline ZnO films doped with B,[10] Al,[10,11] Ga,[10,12,13] and In[10,14] show a strong thickness dependence of electrical properties up to a film thickness of ~4000 Å.

Fortunately, the optical response of free electrons in the TCO's can be expressed successfully by the simple Drude model.[6,7] Moreover, from the analysis of free-carrier absorption using the Drude model, carrier concentration, mobility, and conductivity can be deduced without the requirement of forming metal electrodes on samples.[42–44] In multilayered structures, the characterization of each conductive layer becomes possible.[45] From a real-time measurement of free-carrier absorption, the dynamics of carrier generation during thin-film growth can be determined.[44] Thus, the assessment of free-carrier absorption is quite important not only for the physical understanding of free-carrier absorption but also for the optical conductivity measurement.

An important phenomenon that has been observed in the highly doped TCO's is an increase in effective mass m^*.[5,6,11,16–25] Although m^* can be extracted from the dielectric function determined experimentally, m^* reported for doped ZnO (Refs. 11 and 16–18) and In_2O_3:Sn (Refs. 5, 6, and 19–24) differs significantly. Furthermore, several studies for doped ZnO (Refs. 18 and 25) and In_2O_3:Sn (Refs. 21–24) showed different variations of m^* with carrier concentration. In the TCO's, therefore, m^* remains highly controversial and needs to be determined accurately. On the other hand, when the carrier concentration and mobility are

estimated optically from free carrier absorption, m^* is required in the analysis.[42–44] Thus, the variation of m^* with carrier concentration can best be examined by comparing carrier concentrations obtained electrically with those obtained optically from free carrier absorption.

So far, in spite of the growing importance of the TCO's, the optical constants of doped ZnO and In_2O_3:Sn have not been studied extensively. In particular, for the variation of the optical constants with carrier concentration, only a few studies have been made.[6,7,11] Moreover, most of the optical constants reported so far have been obtained from rather thick samples (1000–5000 Å) using transmittance/reflectance (T/R) measurements.[6,7,11,14,16,23] As mentioned earlier, the optical properties of the TCO's generally vary with film thickness, and a simple T/R analysis assuming uniform optical constants toward growth direction may lead to serious errors in estimating the optical constants.

Compared with T/R measurement, spectroscopic ellipsometry (SE) allows the straightforward measurement of optical constants, since the two values of optical constants can be obtained directly from two independent ellipsometry parameters (Ψ, Δ).[46] In the SE analysis, the variation of optical constants with film thickness can be incorporated explicitly.[26,29] SE further enables us to measure optical constants of very thin films with high precision. Thus, SE becomes quite useful when thin TCO films are characterized to avoid the thickness variation of the optical constants. So far, several SE studies have been reported for doped ZnO (Refs. 34–36) and In_2O_3:Sn (Refs. 26–33).

In this study, we have determined the dielectric functions of ZnO:Ga and In_2O_3:Sn with different carrier concentrations by SE, in an attempt to investigate effects of carrier concentration on the dielectric function of the TCO's. To suppress analysis errors arising from the thickness variation of the optical constants, thin TCO films (~700 Å) were characterized. From the analysis of the dielectric function, we determined m^* for the TCO's. The m^* in the TCO's was found to increase linearly with increasing carrier concentration. In order to find the validity of the SE analysis, we further compared carrier transport properties obtained from SE with those characterized by Hall measurement. As a result, we found excellent agreement between carrier concentrations determined by SE and Hall measurements.

II. EXPERIMENT

We prepared ZnO:Ga and In_2O_3:Sn thin films (~700 Å) at different deposition temperatures from 25 to 240 °C by magnetron sputtering. The sputtering depositions were performed at an Ar gas pressure of 1 mTorr using a dc power of 200 W (ZnO:Ga) and an rf power of 100 W (In_2O_3:Sn). For the ZnO:Ga deposition, we used ZnO targets that have different Ga_2O_3 contents in a range from 0.5 to 5.7 wt %,[37] whereas the In_2O_3:Sn thin films were prepared using a In_2O_3 target with a fixed SnO_2 content of 10 wt %.

The electrical properties of the TCO films were obtained from ac-Hall measurements in the van der Pauw configuration. For the Hall measurement, we formed Al electrodes on the samples. In the analyses, film thicknesses determined by SE were used. The SE spectra (Ψ, Δ) were measured in a range from 0.7 to 5.0 eV at room temperature using a rotating-compensator instrument (J. A. Woollam, M-2000). Since the TCO's are essentially transparent materials, the Δ values in the SE spectra vary in a wide region of $-180° < \Delta \leqslant 180°$. Nevertheless, in a rotating-analyzer (polarizer) ellipsometer, which has been used more commonly, measurement errors increase drastically when Δ approaches to 0° and 180°.[47] Thus, for an accurate measurement of the TCO's, application of the rotating-compensator ellipsometer is quite important.

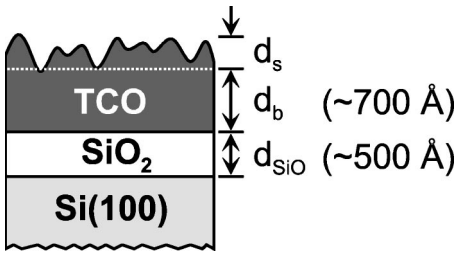

FIG. 1. Optical model used for transparent conductive oxide (TCO) thin films formed on SiO_2/Si(100) substrates. The thicknesses for surface roughness layer, bulk layer, and SiO_2 layer are denoted as d_s, d_b, and d_{SiO}, respectively. The rear surface of the Si(100) substrate was roughened to eliminate back-side light reflection.

III. SE ANALYSIS

Figure 1 shows an optical model used in SE analyses. When the TCO's are formed on glass substrates, complications arise in the SE analysis by the effect of back-surface light reflection.[48–50] Thus, we prepared the TCO thin film on a Si(100) substrate covered with a thermal oxide layer (~500 Å). This SiO_2 layer was provided to perform the electrical measurement of the TCO film. To eliminate the back-surface reflection that still occurs at <1.2 eV in Si,[49] rear surfaces of the Si(100) substrates were roughened.

In Fig. 1, d_s, d_b, and d_{SiO} indicate the thicknesses for surface roughness layer, bulk layer, and SiO_2 layer, respectively. To simplify the SE analysis, we determined d_{SiO} from SE prior to the TCO deposition using dielectric functions reported previously.[51] We modeled the dielectric function of the surface roughness layer as a 50/50 vol % mixture of the TCO bulk layer and voids, applying Bruggeman effective-medium theory.[52,53] The dielectric function of the TCO bulk layer was modeled by combining the Drude model with the Tauc-Lorentz (TL) model.[54] The TL model has been confirmed to provide excellent fitting to experimental data in various TCO's including SnO_2 (Ref. 54) and ZnO (Ref. 36). Several other studies have reported dielectric function modeling by the Lorentz oscillator model,[27,28,31,33,34] Cauchy model,[28,32] and Forouhi-Bloomer model,[30] instead of the TL model. Here, we applied the TL model to determine d_s and d_b.

In our model, the dielectric function of the TCO, $\varepsilon(E) = \varepsilon_1(E) - i\varepsilon_2(E)$, is expressed by

$$\varepsilon(E) = \varepsilon_{\mathrm{TL}}(E) + \varepsilon_{\mathrm{D}}(E), \tag{1}$$

where $\varepsilon_{\mathrm{TL}}(E)$ and $\varepsilon_{\mathrm{D}}(E)$ indicate the dielectric functions calculated by the TL and Drude models, respectively. In the TL model, the dielectric function is obtained from five parameters $\{A_{\mathrm{TL}}, C, E_{\mathrm{T}}, E_0, \varepsilon_1(\infty)\}$, which represent the amplitude, broadening parameter, Tauc optical gap, peak transition energy, and energy-independent contribution to $\varepsilon_1(E)$, respectively.[55]

The expression for $\varepsilon_{\mathrm{D}}(E)$ is given by

$$\varepsilon_{\mathrm{D}}(E) = -\frac{A_{\mathrm{D}}}{E^2 - i\Gamma_{\mathrm{D}}E} = \left(-\frac{A_{\mathrm{D}}}{E^2 + \Gamma_{\mathrm{D}}^2}\right) - i\left(\frac{A_{\mathrm{D}}\Gamma_{\mathrm{D}}}{E^3 + \Gamma_{\mathrm{D}}^2 E}\right), \tag{2}$$

where the two parameters $(A_{\mathrm{D}}, \Gamma_{\mathrm{D}})$ show the amplitude and broadening parameter. In the Drude theory, A_{D} is expressed by

$$A_{\mathrm{D}} = \varepsilon_\infty E_{\mathrm{p}}^2, \tag{3}$$

$$E_{\mathrm{p}} = \hbar\omega_{\mathrm{p}} = \left(\frac{\hbar^2 e^2 N_{\mathrm{opt}}}{m^* \varepsilon_\infty \varepsilon_0}\right)^{1/2}. \tag{4}$$

Here, ε_∞ and E_{p} indicate the high-frequency dielectric constant and plasma energy, respectively. In Eq. (4), ω_{p}, e, N_{opt}, and ε_0 show the plasma angular frequency, electron charge, optical carrier concentration, and free-space permittivity, respectively.

On the other hand, Γ_{D} in Eq. (2) is given by

$$\Gamma_{\mathrm{D}} = \hbar\gamma = \frac{\hbar e}{m^* \mu_{\mathrm{opt}}}, \tag{5}$$

where γ and μ_{opt} denote the broadening parameter in angular frequency and optical mobility, respectively. From the two parameters $(A_{\mathrm{D}}, \Gamma_{\mathrm{D}})$, N_{opt} and μ_{opt} can be deduced if m^* is known. The optical conductivity of the films is also obtained from $\sigma_{\mathrm{opt}} = eN_{\mathrm{opt}}\mu_{\mathrm{opt}}$.

At sufficiently low energies, the real part of $\varepsilon_{\mathrm{TL}}(E)$ shows the constant value of ε_∞. At this condition, $\varepsilon_1(E)$ can be written as

$$\varepsilon_1(E) = \varepsilon_\infty - \frac{A_{\mathrm{D}}}{E^2 + \Gamma_{\mathrm{D}}^2}. \tag{6}$$

Thus, by plotting ε_1 versus $1/(E^2 + \Gamma_{\mathrm{D}}^2)$, ε_∞ can be determined from an intercept.[56,57]

IV. RESULTS AND DISCUSSION

A. Dielectric functions of ZnO:Ga and In_2O_3:Sn

Figure 2 shows (a) Hall carrier concentration N_{Hall} and (b) Hall mobility μ_{Hall} of the TCO thin films, plotted as functions of the deposition temperature T_{depo}. Although the obtained results do not vary systematically, we found increases in N_{Hall} with increasing T_{depo}. For the ZnO:Ga, N_{Hall} also increases as the Ga_2O_3 content in the ZnO targets increases from 0.5 to 5.7 wt %, as reported previously.[12,37] In Fig. 2(b), the ZnO:Ga films show lower mobility, compared with

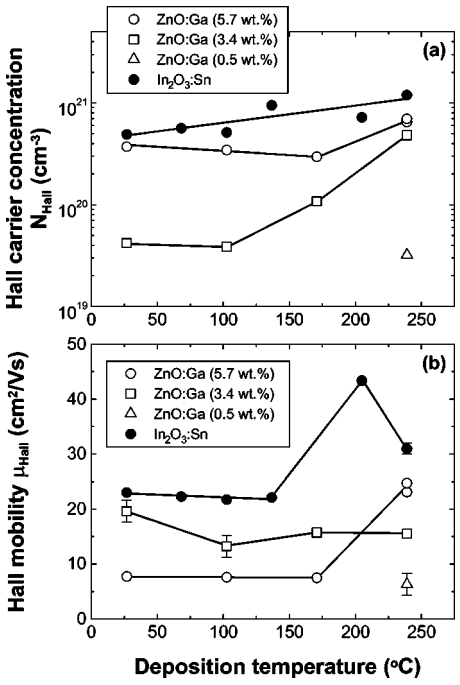

FIG. 2. (a) Hall carrier concentration N_{Hall} and (b) Hall mobility μ_{Hall} of ZnO:Ga and In_2O_3:Sn, plotted as functions of deposition temperature. In the ZnO:Ga depositions, the Ga_2O_3 content in ZnO targets was varied from 0.5 to 5.7 wt %.

the In_2O_3:Sn films. We performed the SE analyses for the samples shown in Fig. 2.

Figure 3 shows the SE spectra for (a) ZnO:Ga and (b) In_2O_3:Sn thin films deposited at 240 °C in Fig. 2. The SE spectra in Fig. 3 were measured at an incidence angle of 70.6°. In the SE spectra, only one out of every three data points is shown for clarity. The peak position of Ψ observed at $E \sim 2$ eV represents the TCO film thickness and shifts toward lower energies with increasing film thickness. The spectral features observed at $E < 1.5$ eV arise from free-carrier absorption. At $E > 3.5$ eV, on the other hand, large differences can be seen between ZnO:Ga and In_2O_3:Sn due to differences in band structures.

The solid lines in Fig. 3 show the calculation results obtained from linear regression analyses. To avoid complicated structures observed in the dielectric functions at higher energies,[6,7,35] we performed the fitting at $E < 3.5$ eV. The analysis parameters obtained from the fitting are summarized in Table I. In the analyses, a fixed value of $\varepsilon_1(\infty) = 1$ was used. Thus, we performed the fitting using $\{d_{\mathrm{s}}, d_{\mathrm{b}}, A_{\mathrm{D}}, \Gamma_{\mathrm{D}}, A_{\mathrm{TL}}, C, E_{\mathrm{T}}, E_0\}$ as free parameters. In the fitting, the parameters A_{D} and A_{TL} show relatively large correlations with the broadening parameters Γ_{D} and C, respectively. The values of cross-correlation parameters between the Drude model $(A_{\mathrm{D}}, \Gamma_{\mathrm{D}})$ and the TL model $\{A_{\mathrm{TL}}, C, E_{\mathrm{T}}, E_0\}$, however, are low enough to determine these sets of the parameters accurately. As shown in Fig. 3, our model provides excellent fitting to the experimental spectra in a wide energy region.

As shown in Table I, the thickness parameters $(d_{\mathrm{s}}, d_{\mathrm{b}}, d_{\mathrm{SiO}})$ can be determined from SE. When each thickness in the optical model is known, the dielectric function

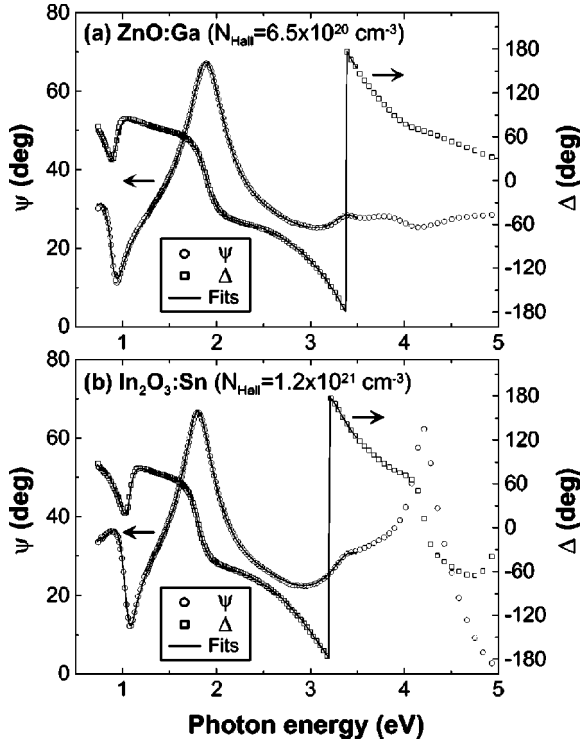

FIG. 3. SE spectra measured for (a) ZnO:Ga and (b) In_2O_3:Sn thin films deposited at 240 °C. The angle of incidence in the SE measurement is 70.6°. In the SE spectra, only one out of every three data points is shown for clarity. Solid lines show fitting results.

TABLE I. Best-fit parameters extracted from the dielectric function modeling using the Drude model (A_D, Γ_D) and Tauc-Lorentz model $\{A_{TL}, C, E_T, E_0, \varepsilon_1(\infty)\}$. The errors of extracted parameters show uncorrelated 90% confidence limits. The results were obtained from the ZnO:Ga (Ga_2O_3 content: 5.7 wt %) and In_2O_3:Sn thin films deposited at 240 °C. The χ^2 and E_p show final fitting quality (biased estimator) and plasma energy determined experimentally from the dielectric functions, respectively. The Hall carrier concentration N_{Hall} and Hall mobility μ_{Hall} are also indicated.

	ZnO:Ga (5.7 wt %)	In_2O_3:Sn
d_s (Å)	41.3±1.9	35.8±1.6
d_b (Å)	605.6±1.4	685.7±1.2
d_{SiO} (Å)	519.4±0.1	516.4±0.1
A_D (eV)	2.537±0.005	3.786±0.007
Γ_D (eV)	0.130±0.001	0.102±0.001
A_{TL} (eV)	139.4±1.4	111.4±7
C (eV)	15.0±3	11.7±2
E_T (eV)	3.14±0.01	3.13±0.02
E_0 (eV)	7.3±0.1	9.6±0.2
$\varepsilon_1(\infty)$	1 (fixed)	1 (fixed)
χ^2	17.20	11.26
E_p (eV)	0.837	0.970
N_{Hall} (cm^{-3})	$(6.48\pm0.06)\times10^{20}$	$(1.20\pm0.01)\times10^{21}$
μ_{Hall} [cm^2/(V s)]	23.1±0.2	31.0±1

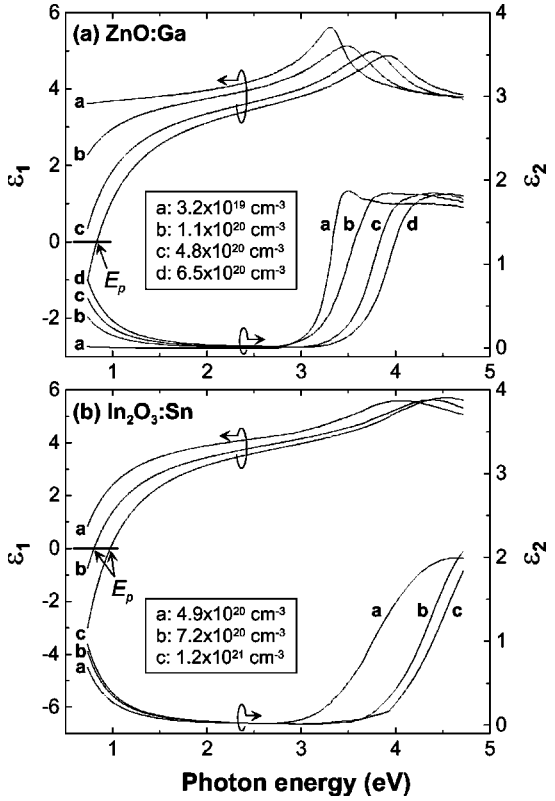

FIG. 4. Dielectric functions of (a) ZnO:Ga and (b) In_2O_3:Sn obtained from SE analyses. The dielectric functions were extracted from the TCO films that have different carrier concentrations. In the figure, Hall carrier concentration N_{Hall} of each sample is indicated as $a-d$ in (a) and $a-c$ in (b). The $E_p=\hbar\omega_p$ in the figure shows plasma energy defined by the photon energy where $\varepsilon_1(E)=0$.

can be extracted directly from the measured SE spectra by mathematical inversion using Fresnel equations.[58] Figure 4 summarizes the dielectric functions of (a) ZnO:Ga and (b) In_2O_3:Sn extracted from the mathematical inversion. At $E<3.0$ eV, however, the dielectric functions calculated by Eq. (1) are shown to eliminate spectral noise that appears at lower energies. The dielectric functions in Fig. 4 were obtained from the samples having different carrier concentrations and N_{Hall} of each sample is indicated in the figure.

In the dielectric functions shown in Fig. 4, the ε_1 peaks at ~3 eV show clear shifts toward higher energies with increasing N_{Hall} due to the Burstein-Moss effect. At lower energies, on the other hand, the ε_2 values increase with increasing N_{Hall} by the effect of free carrier absorption. It can be seen that the slight increase in free-carrier absorption leads to the significant reduction in ε_1. As indicated in Fig. 4, the value of E_p can be obtained experimentally from the energy position where $\varepsilon_1(E)=0$.

As reported earlier,[59–61] the ε_1 and ε_2 peaks in ZnO originate from excitonic transition. The ε_1 peak of the ZnO:Ga in Fig. 4, however, indicates enhanced broadening as N_{Hall} increases. In general, the broadening parameter of a transition peak is inversely proportional to the lifetime of carriers or excitons.[62,63] Thus, this result implies that the lifetime of excitons becomes shorter as the electron concentration increases. Such an effect has been explained by the screening

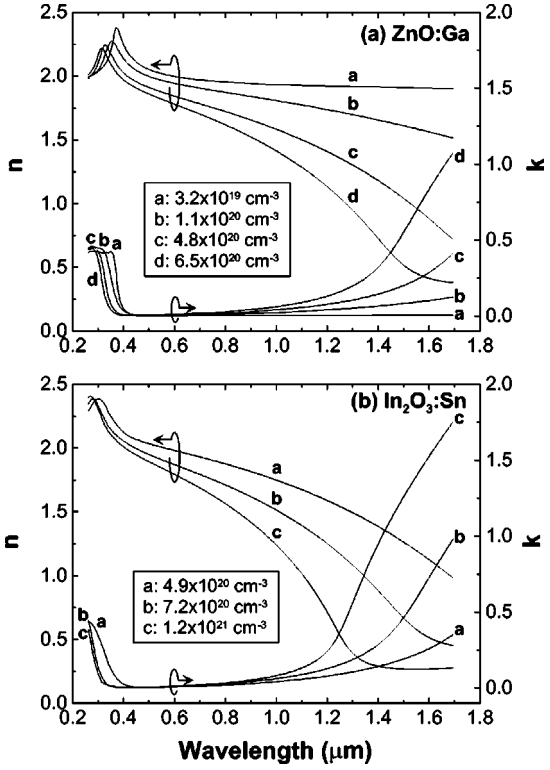

FIG. 5. (n,k) spectra of (a) ZnO:Ga and (b) In_2O_3:Sn obtained from dielectric functions shown in Fig. 4. In the figure, Hall carrier concentration N_{Hall} of each sample is indicated as $a-d$ in (a) and $a-c$ in (b).

of the Coulomb potential;[58,64] in other words, the Coulomb attraction in an electron-hole pair is screened by free electrons surrounding the exciton, reducing the stability of the exciton.

Since spectra for refractive index n and extinction coefficient k have been used widely in device designing, (n,k) spectra of the TCO's are also shown in Fig. 5. These results have been obtained from simple data conversion using the dielectric functions shown in Fig. 4. In Fig. 5, the reduction in n and increase in k by free-carrier absorption can be seen more clearly.

B. Analysis of dielectric function

Figure 6 shows ε_1 of the ZnO:Ga, plotted as a function of $1/(E^2+\Gamma_D^2)$. Solid lines indicate linear fits to the experimental results. As shown in Eq. (6), ε_∞ can be obtained from the intercept at $1/(E^2+\Gamma_D^2)=0$.[56,57] In this analysis, we used Γ_D extracted from the SE analysis. The Γ_D values, however, are rather small ($\Gamma_D \sim 0.1$ eV), compared with E, and similar ε_∞ values can also be obtained by plotting ε_1 versus $1/E^2$ (Refs. 6 and 7). As shown in Fig. 6, ε_1 varies linearly versus $1/(E^2+\Gamma_D^2)$, indicating the validity of the Drude theory. For $N_{Hall}=6.5\times10^{20}$ cm^{-3}, however, the linear fit deviates slightly around $\varepsilon_1 \sim 0$. This result indicates that the variation in ε_1 differs slightly from the Drude model at around E_p. It can be seen clearly that ε_∞ decreases with increasing N_{Hall}. Similar plots have been obtained for the In_2O_3:Sn. It should

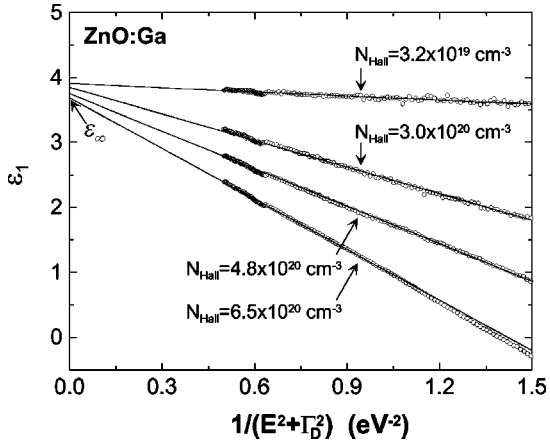

FIG. 6. Real part of dielectric function for ZnO:Ga, plotted as a function of $1/(E^2+\Gamma_D^2)$. The Γ_D is a broadening parameter expressed by Eq. (5). In the figure, Hall carrier concentration N_{Hall} of each sample is shown. The high frequency dielectric constant ε_∞ can be obtained from the intercept at $1/(E^2+\Gamma_D^2)=0$.

be mentioned that ε_∞ can also be obtained from the TL model using the parameters $\{A_{TL}, C, E_T, E_0, \varepsilon_1(\infty)\}$. In this case, ε_∞ is simply determined from the real part of $\varepsilon_{TL}(E)$ at low energies. The ε_∞ values obtained by the analyses, however, are similar to those determined from the plots shown in Fig. 6.

Figure 7 shows ε_∞ obtained from the analysis, plotted as a function of N_{Hall}. We find that ε_∞ of ZnO:Ga and In_2O_3:Sn decreases linearly with increasing N_{Hall}. The reduction in ε_∞ for the ZnO:Ga, however, is slightly smaller than that for the In_2O_3:Sn. Our results shown in Fig. 7 are strong contrasts to previous reports.[6,7,21–23] For doped ZnO, Jin *et al.* reported a constant value of $\varepsilon_\infty=3.85\pm0.1$ irrespective of the carrier concentration in a range from 0.95×10^{20} to 4.5×10^{20} cm^{-3} (Ref. 7). For In_2O_3:Sn, a constant value of $\varepsilon_\infty=4$ has also been reported,[6,21] whereas other studies reported relatively large reductions in ε_∞ from 4 to 3.[22,23] In these studies, however, ε_∞ was determined from thick samples

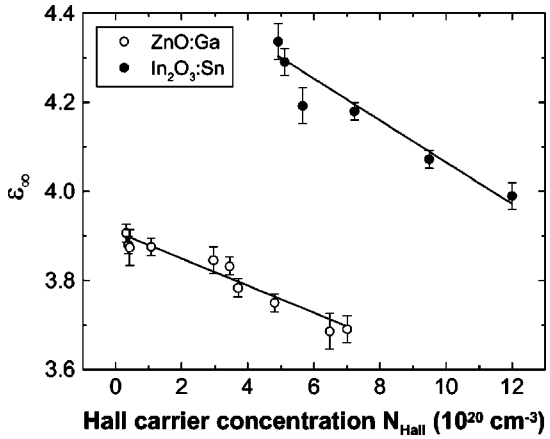

FIG. 7. High-frequency dielectric constant ε_∞ of ZnO:Ga and In_2O_3:Sn, plotted as a function of Hall carrier concentration N_{Hall}. These values have been estimated from the dielectric function analysis shown in Fig. 6.

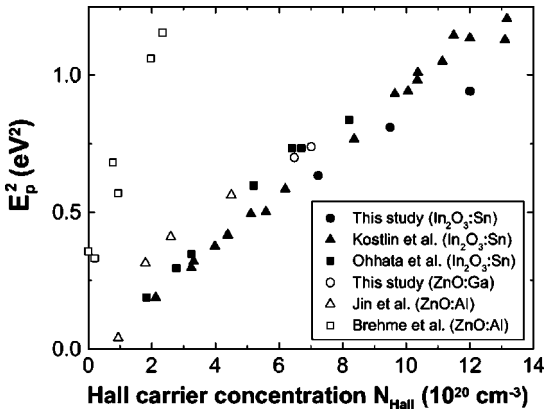

FIG. 8. E_p^2 of doped ZnO and In_2O_3:Sn, plotted as a function of Hall carrier concentration N_{Hall}. The plasma energy $E_p=\hbar\omega_p$ was determined from the dielectric function. In the figure, experimental results reported previously by Kostlin *et al.* (Ref. 20), Ohhata *et al.* (Ref. 22), Jin *et al.* (Ref. 7), and Brehme *et al.* (Ref. 17) are also shown.

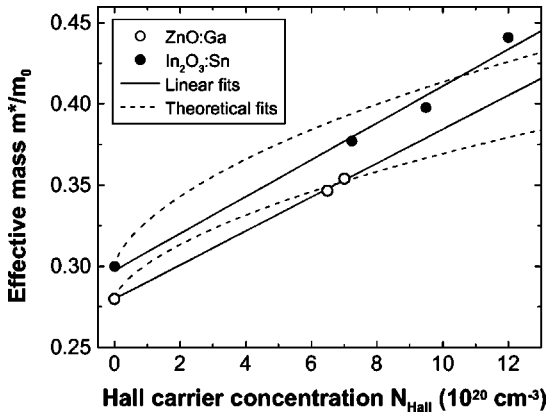

FIG. 9. Effective mass m^*/m_0 of ZnO:Ga and In_2O_3:Sn, plotted as a function of Hall carrier concentration N_{Hall}. The m_0 denotes the free-electron mass. Solid lines indicate linear fits to the experimental data. These fitting lines are expressed by Eqs. (7) and (8). Dotted lines show calculation results using the theoretical model given by Eq. (9).

(1000–5000 Å) using the simple T/R analysis. Thus, the variation of the optical constants with film thickness may have affected their experimental results.

Figure 8 shows E_p^2 plotted as a function of N_{Hall}. Due to the limited energy region for the SE measurement, only five data points were obtained in our study. For comparison, the E_p^2 values reported for doped ZnO (Refs. 7 and 17) and In_2O_3:Sn (Refs. 20 and 22) are also shown in Fig. 8. For doped ZnO, the variation of E_p^2 with N_{Hall} observed in this study is similar to that reported by Jin *et al.*,[7] but is different from that obtained by Brehme *et al.*[17] For In_2O_3:Sn, the E_p^2 values determined in this study show reasonable agreement with those reported by Kostlin *et al.*,[20] but are smaller than those obtained by Ohhata *et al.*[22] As confirmed from Eq. (4), E_p^2 becomes zero when there are no free carriers. Thus, the result reported from Brehme *et al.* appears to include relatively large errors.

If the values of the three parameters (N_{opt}, ε_∞, E_p) are known, m^* of the TCO's can be obtained directly from Eq. (4). Thus, assuming $N_{opt}=N_{Hall}$, we determined m^* of ZnO:Ga and In_2O_3:Sn. In the calculation, we used ε_∞ and E_p shown in Figs. 7 and 8, respectively. Figure 9 shows m^*/m_0 obtained from this procedure, plotted as a function of N_{Hall}. Here, m_0 denotes the free-electron mass. At $N_{Hall}=0$, we show the reported values of $m^*(\mathrm{ZnO})=0.28m_0$ (Ref. 38) and $m^*(\mathrm{In_2O_3})=0.30m_0$ (Ref. 5). As shown in Fig. 9, m^* shows distinct increases with N_{Hall}.

So far, several other studies have also reported the increase in m^* with carrier concentration.[18,21–25] In addition, the reduction in μ_{Hall} observed for doped ZnO at high N_{Hall} ($>4\times10^{20}$ cm^{-3}) has been explained by the increase in m^* (Ref. 39). In contrast to previous studies,[18,21–25] however, we found that m^* of the ZnO:Ga and In_2O_3:Sn increases linearly with increasing N_{Hall}. It should be emphasized that m^* has a strong relationship with ε_∞, as confirmed from Eq. (4). In particular, if E_p^2 increases linearly versus N_{Hall}, m^* should change according to the variation of ε_∞, as long as the experimental data follows the Drude theory. Thus, the linear reductions in ε_∞ shown in Fig. 7 can be correlated with the linear increases in m^*. Although uncertainty remains concerning the linearity of m^*(ZnO) owing to the small number of the data points, the linear reduction in ε_∞ supports the linear increase in m^*.

From linear fits to the experimental data shown in Fig. 9, we determined the variation of m^* with N_{Hall} as

$$m^*(\mathrm{ZnO}) = (0.280 + 0.010\times10^{-20}N_{Hall})m_0, \quad (7)$$

$$m^*(\mathrm{In_2O_3{:}Sn}) = (0.297 + 0.011\times10^{-20}N_{Hall})m_0. \quad (8)$$

As confirmed from the above equations, the slopes for the ZnO and In_2O_3:Sn are rather similar. Compared with other studies,[18,25] m^*(ZnO) obtained in this study shows smaller values. For In_2O_3:Sn, our result is rather similar to the result reported by Clanget,[21] whereas other studies reported higher or lower values for the variation of m^* with N_{Hall}.[22–24] The increase in m^* has also been observed for other TCO's.[40,56]

The increase in m^* observed in the heavily doped TCO's has been explained by the influence of the degeneracy and the nonparabolicity of the TCO conduction band.[17,18,21–25,38–40] According to a theoretical model that assumes the nonparabolic conduction band,[40] m^* at Fermi level is given by

$$m^* = m_0^*\left\{1 + 2P\frac{\hbar^2}{m_0^*}(3\pi^2N_{opt})^{2/3}\right\}^{1/2}, \quad (9)$$

where m_0^* and P are the effective mass at the bottom of the conduction band and nonparabolicity parameter, respectively. Dotted lines in Fig. 9 show the result of the theoretical fitting by Eq. (9). From the fitting, P for the ZnO:Ga and In_2O_3:Sn was determined to be 0.142 eV^{-1} and 0.180 eV^{-1}, respectively. For the In_2O_3:Sn, however, m^* calculated by this model shows rather poor agreement with m^* obtained experimentally, suggesting that this model is too simple to express the nonparabolicity of the TCO conduction band.

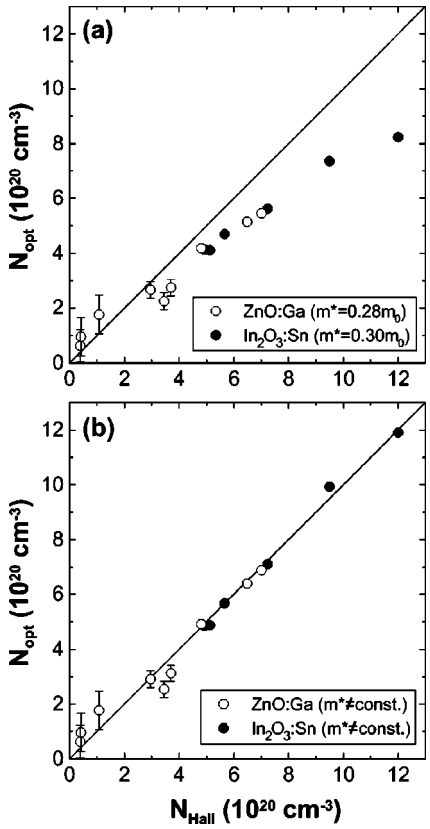

FIG. 10. Optical carrier concentration N_{opt} obtained from the SE analyses using (a) $m^*(\mathrm{ZnO})=0.28m_0$ and $m^*(\mathrm{In_2O_3:Sn})=0.30m_0$ and (b) $m^*(\mathrm{ZnO})$ given by Eq. (7) and $m^*(\mathrm{In_2O_3:Sn})$ given by Eq. (8), plotted as functions of Hall carrier concentration N_{Hall}.

In a few studies, m^* of doped ZnO (Ref. 17) and In_2O_3:Sn (Refs. 6 and 20) was obtained assuming $\varepsilon_\infty=4$. In this case, a single value of m^* is determined from the slope of the plot shown in Fig. 8. Nevertheless, this assumption is not valid, as confirmed from our result shown in Fig. 7. Thus, m^* deduced assuming $\varepsilon_\infty=4$ includes large errors.

C. Correlation with Hall measurement

In order to find the validity of our analyses, we compared N_{opt} and μ_{opt} determined by SE with N_{Hall} and μ_{Hall}, respectively. As mentioned earlier, N_{opt} can be obtained from the two parameters (A_D, m^*) by applying Eqs. (3) and (4). Figure 10 shows N_{opt} obtained from the SE analyses using (a) $m^*(\mathrm{ZnO})=0.28m_0$ and $m^*(\mathrm{In_2O_3:Sn})=0.30m_0$ and (b) $m^*(\mathrm{ZnO})$ given by Eq. (7) and $m^*(\mathrm{In_2O_3:Sn})$ given by Eq. (8), plotted as functions of N_{Hall}. In Fig. 10(a), it can be seen that the difference between N_{opt} and N_{Hall} increases as N_{Hall} increases.

In contrast, when the variation of m^* with carrier concentration is taken into account, N_{opt} shows remarkable agreement with N_{Hall}, as shown in Fig. 10(b). This result confirms the increase in m^* with carrier concentration. It should be noted that N_{opt} of the In_2O_3:Sn shows poorer agreement with N_{Hall} when m^* calculated by Eq. (9) is used, supporting the linear variation of m^* with N_{Hall}. In Sec. IV B, we determined m^* from Eq. (4) assuming $N_{opt}=N_{Hall}$. Obviously, this assumption is valid, as confirmed from the result shown in Fig. 10(b). As mentioned earlier, in order to obtain m^* accurately, the dependence of ε_∞ on N_{Hall} has to be included in the calculation explicitly. Thus, the excellent agreement between N_{opt} and N_{Hall} strongly supports the validity of our analysis results.

At lower carrier concentrations ($N_{Hall}<4\times10^{20}$ cm^{-3}), however, the SE analysis becomes increasingly difficult owing to low free-carrier absorption in the TCO films. Sensitivity for free-carrier absorption can be increased by simply increasing the film thickness, although the thickness variation of the optical constants may cause difficulties in the analysis.

The result of Fig. 10(a) shows that N_{opt} is seriously underestimated when the smaller m^* values are used. A similar result was reported previously for ZnO:Ga.[13] This result can be explained easily from Eqs. (3) and (4). In particular, for a constant A_D value, N_{opt} decreases with decreasing m^* used in the analysis. Unfortunately, the above results show that the analysis of N_{opt} is difficult when the Hall measurement is not performed for the same sample, since we determined m^* from N_{Hall}. Thus, we determined correction coefficients for N_{opt}. To obtain the correction coefficients, we plotted two sets of N_{opt} shown in Fig. 10 and fitted the data points by second-order polynomials. From this analysis, we obtained the relation expressed by

$$N_{opt}=0.917N'_{opt}+0.061\times10^{-20}N'^2_{opt}\ \mathrm{cm}^{-3}. \qquad (10)$$

Here, N'_{opt} shows N_{opt} determined using $m^*(\mathrm{ZnO})=0.28m_0$ and $m^*(\mathrm{In_2O_3:Sn})=0.30m_0$. Thus, true N_{opt} can be calculated from N'_{opt} using Eq. (10).

Figure 11 shows μ_{opt} obtained from the SE analyses using (a) $m^*(\mathrm{ZnO})=0.28m_0$ and $m^*(\mathrm{In_2O_3:Sn})=0.30m_0$ and (b) $m^*(\mathrm{ZnO})$ given by Eq. (7) and $m^*(\mathrm{In_2O_3:Sn})$ given by Eq. (8), plotted as functions of μ_{Hall}. We determined μ_{opt} from the two parameters (Γ_D, m^*) using Eq. (5). As shown in Fig. 11(a), when the values of m^* are fixed, μ_{opt} shows poor agreement with μ_{Hall}. When m^* is varied according to Eqs. (7) and (8), μ_{opt} agrees with μ_{Hall} in a range of μ_{Hall} from 20 to 25 cm^2/(V s). Thus, the agreement between μ_{opt} and μ_{Hall} improves by considering the m^* dependence on the carrier concentration.

In contrast to N_{opt}, μ_{opt} is overestimated when the smaller m^* is used for the calculation, since μ_{opt} increases with decreasing m^*, as confirmed from Eq. (5). If N_{opt} is obtained from Eq. (10), one can estimate m^* of the TCO's from Eqs. (7) and (8). Thus, from this m^*, the true μ_{opt} can also be obtained.

As shown in Fig. 11(b), μ_{opt} shows a constant value of $\sim$25 cm^2/(V s), while μ_{Hall} varies in a range from 5 to 45 cm^2/(V s). Quite interestingly, we find the trends of $\mu_{opt}>\mu_{Hall}$ for ZnO:Ga and $\mu_{opt}<\mu_{Hall}$ for In_2O_3:Sn. It should be emphasized that μ_{opt} estimated from free-carrier absorption represents an average value within grains and does not include the effects of grain boundaries.[42,43] In fact, in microcrystalline Si films, μ_{opt} as determined by free-carrier absorption shows a substantially higher value, com-

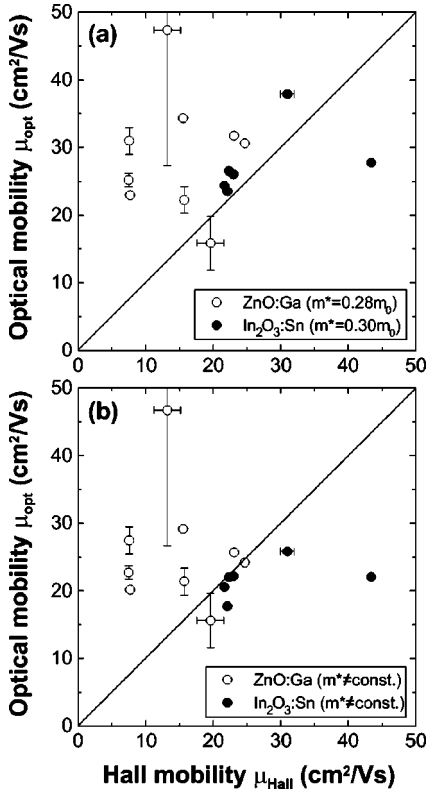

FIG. 11. Optical mobility μ_{opt} obtained from the SE analyses using (a) $m^*(\mathrm{ZnO})=0.28m_0$ and $m^*(\mathrm{In_2O_3:Sn})=0.30m_0$ and (b) $m^*(\mathrm{ZnO})$ given by Eq. (7) and $m^*(\mathrm{In_2O_3:Sn})$ given by Eq. (8), plotted as functions of Hall mobility μ_{Hall}.

pared with the one evaluated by Hall measurement, due to poor carrier transport properties at grain boundaries.[42] Thus, our result shown in Fig. 11(b) indicates that the carrier transports at grain boundaries are different in ZnO:Ga and $\mathrm{In_2O_3:Sn}$.

The trend of $\mu_{opt} > \mu_{Hall}$ observed for ZnO:Ga implies that the carrier transport is hindered by the presence of grain boundaries. In doped ZnO, μ_{Hall} has been reported to decrease at $N_{Hall} < 4\times10^{20}\ \mathrm{cm^{-3}}$ due to grain boundary scattering.[39] At higher carrier concentrations ($>4\times10^{20}\ \mathrm{cm^{-3}}$), however, grain boundary scattering makes a small contribution since electrons tunnel thin potential barriers formed at grain boundaries.[41] In fact, when N_{Hall} of the ZnO:Ga is high enough ($N_{Hall}\sim6\times10^{20}\ \mathrm{cm^{-3}}$), we find $\mu_{opt}\sim\mu_{Hall}$. In these films, electron scattering by ionized impurities dominates the carrier transport.[10,24,39,41]

A similar explanation can also be applied for the $\mathrm{In_2O_3:Sn}$.[21,24] In particular, we find better agreement between μ_{opt} and μ_{Hall} for the $\mathrm{In_2O_3:Sn}$, compared with the ZnO:Ga, due to higher N_{Hall} in the $\mathrm{In_2O_3:Sn}$. For the $\mathrm{In_2O_3:Sn}$ deposited at high temperatures ($T_{depo} > 200\ ^\circ\mathrm{C}$ in Fig. 2), we observe $\mu_{opt} < \mu_{Hall}$. Although details are not clear, we suggest enhanced carrier transport in these films by percolation of the large polycrystalline grains formed at high T_{depo}.

D. Analysis of band-edge absorption

In a band-edge absorption region, the absorption coefficient α of the TCO's is approximated by $\alpha=A(E-E_g)^{1/2}$.

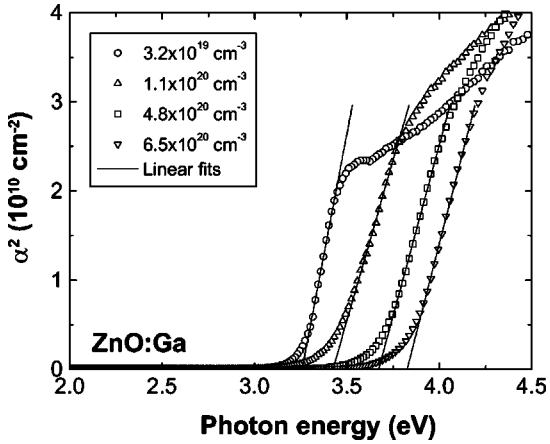

FIG. 12. Square of absorption coefficient α^2 obtained for ZnO:Ga, plotted as a function of photon energy. In the figure, Hall carrier concentration N_{Hall} of each sample is indicated. Solid lines show linear fits to the experimental data. The intercept at $\alpha^2=0$ shows a band gap of the ZnO:Ga.

Thus, the optical band gap E_g of the TCO's can be estimated by plotting α^2 versus photon energy.[11,22] Figure 12 shows α^2 versus photon energy for the ZnO:Ga. We obtained the α spectra from the k spectra shown in Fig. 5(a) using $\alpha=4\pi k/\lambda$. In Fig. 12, a fundamental absorption edge shifts toward higher energies with increasing N_{Hall} by the Burstein-Moss effect. Solid lines show linear fits to the experimental data and E_g was estimated from the intercept at $\alpha^2=0$. As pointed out previously,[6] however, this analysis is not applicable for heavily doped TCO's, since the conduction band is not parabolic anymore due to the conduction band filling with electrons. To determine E_g accurately, theoretical treatments are necessary.[6] Here, we estimated E_g from the conventional method for comparison with other studies.

The shift of E_g by the Burstein-Moss effect is expressed by

$$\Delta E_g = \frac{\hbar^2}{2m^*_{eh}}(3\pi^2 N_{opt})^{2/3}, \tag{11}$$

where m^*_{eh} is reduced effective mass given by $(m^*_{eh})^{-1}=(m^*_e)^{-1}+(m^*_h)^{-1}$ (Ref. 6). The m^*_e and m^*_h denote the effective mass for the electron and hole, respectively. According to the Burstein-Moss theory described in Eq. (11), E_g shifts linearly with $N^{2/3}_{opt}$. Figure 13 shows E_g obtained from the analysis shown in Fig. 12, plotted as a function of $N^{2/3}_{Hall}$. A similar result has been obtained when E_g is plotted versus N_{opt}, since $N_{Hall}\sim N_{opt}$. As shown in Fig. 13, E_g increases with $N^{2/3}_{Hall}$. Nevertheless, our result obtained for the ZnO:Ga shows poor agreement with the result reported earlier.[11] Moreover, we found rather high E_g for the $\mathrm{In_2O_3:Sn}$ at $N^{2/3}_{Hall} < 8\times10^{13}\ \mathrm{cm^{-2}}$, compared with other studies.[6]

Although band-gap widening by the Burstein-Moss effect can be calculated from Eq. (11), the actual shift of E_g does not follow this equation. This effect has been interpreted by band-gap shrinkage that occurs simultaneously with band-gap widening.[6,8] The band-gap shrinkage is caused by many-body effects including electron-electron and electron-ion

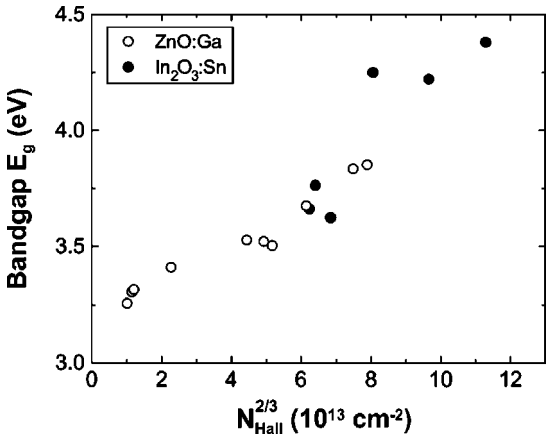

FIG. 13. Band gap E_g of ZnO:Ga and In_2O_3:Sn, plotted as a function of Hall carrier concentration N_{Hall} to the power 2/3.

scatterings.[8] When the band-gap widening by the Burstein-Moss effect and the band-gap narrowing by the many-body effects are considered, the calculated band-gap shift has been reported to show quite good agreement with a shift observed in experiment.[6,8]

E. Construction of the optical database

Our results show clearly that the effects of free carrier absorption in the TCO's can be expressed fully by the simple Drude model. Accordingly, in a low-energy region well below the fundamental absorption edge ($E<2$ eV), the optical constants can be modeled by the three parameters (ε_∞, A_D, Γ_D). In this case, the optical constants are obtained from Eq. (1) assuming $\varepsilon_{TL}(E)=\varepsilon_\infty$. When the results shown in Figs. 7 and 9 are applied, the optical constants are calculated from the two parameters (N_{opt}, μ_{opt}). The modeling can be simplified further assuming a constant μ_{opt} of $\sim 25\ cm^2/(V\ s)$.

Unfortunately, dielectric function modeling in the band-edge absorption region is rather difficult, as the dielectric functions show the complicated structures in this region. Nevertheless, a dielectric function model that can be applied to heavily doped ZnO has been developed recently.[64] By applying this model, the dielectric function of doped ZnO has been parametrized using a total of nine parameters.[35] In addition, the parametrization of the In_2O_3:Sn dielectric function using two Lorentz models has also been reported.[33] Thus, the optical database of the TCO's could be constructed from these parametrization schemes.

V. CONCLUSION

The dielectric functions of ZnO:Ga and In_2O_3:Sn with different carrier concentrations have been obtained by applying spectroscopic ellipsometry. To minimize analysis errors that arise from thickness variation of optical constants, we characterized thin films ($\sim$700 Å). The dielectric function of the transparent conductive oxide was modeled using the classical Drude model combined with the Tauc-Lorentz model. Using the thickness determined by the model, the dielectric functions of the TCO's have been extracted successfully by mathematical inversion. From the dielectric function analyses, high-frequency dielectric constant ε_∞ and plasma energy E_p are deduced. From these values determined experimentally, effective mass m^* of the TCO's is determined. Compared with earlier studies, m^* obtained in this study shows smaller values. We find linear reductions in ε_∞ and linear increases in m^* as the carrier concentration of the ZnO:Ga and In_2O_3:Sn increases. The effects of carrier concentration on the dielectric function of the TCO's can be categorized into three factors including (i) an increase in free-carrier absorption with carrier concentration, (ii) a shift of band-edge absorption by the Burstein-Moss effect, and (iii) a reduction in ε_∞ with increasing carrier concentration. We further characterized the optical carrier concentration and mobility from the SE analyses using the Drude model. The validity of our analyses has been confirmed from the excellent agreement between carrier concentrations determined by SE and Hall measurements. The optical mobility of the TCO's, however, shows poor agreement with the Hall mobility. We attributed this effect to the presence of grain boundaries that affect the Hall mobility significantly, but not the optical mobility.

*Author to whom correspondence should be addressed. Electronic address: hiro-fujiwara@aist.go.jp

[1] B. Rech and H. Wagner, Appl. Phys. A: Mater. Sci. Process. **69**, 155 (1999).
[2] M. Zeman, R. A. C. M. M. van Swaaij, J. W. Metselaar, and R. E. I. Schropp, J. Appl. Phys. **88**, 6436 (2000).
[3] A. S. Ferlauto, G. M. Ferreira, J. M. Pearce, C. R. Wronski, R. W. Collins, X. Deng, and G. Ganguly, J. Appl. Phys. **92**, 2424 (2002).
[4] For a review, see K. L. Chopra, S. Major, and D. K. Pandya, Thin Solid Films **102**, 1 (1983).
[5] For a review, see Z. M. Jarzebski, Phys. Status Solidi A **71**, 13 (1982).
[6] For a review, see I. Hamberg and C. G. Granqvist, J. Appl. Phys. **60**, R123 (1986).
[7] Z.-C. Jin, I. Hamberg, and C. G. Granqvist, J. Appl. Phys. **64**, 5117 (1988).
[8] B. E. Sernelius, K.-F. Berggren, Z.-C. Jin, I. Hamberg, and C. G. Granqvist, Phys. Rev. B **37**, 10 244 (1988).
[9] Y. Shigesato, S. Takaki, and T. Haranou, Appl. Surf. Sci. **48/49**, 269 (1991).
[10] T. Minami, H. Sato, H. Nanto, and S. Takata, Jpn. J. Appl. Phys., Part 2 **24**, L781 (1985).
[11] Y. Qu, T. A. Gessert, K. Ramanathan, R. G. Dhere, R. Noufi, and T. J. Coutts, J. Vac. Sci. Technol. A **11**, 996 (1993).
[12] B. H. Choi, H. B. Im, J. S. Song, and K. H. Yoon, Thin Solid Films **193–194**, 712 (1990).
[13] J. Hu and R. G. Gordon, J. Appl. Phys. **72**, 5381 (1992).

[14] S. Major, A. Banerjee, and K. L. Chopra, Thin Solid Films **125**, 179 (1985).
[15] A. P. Roth, J. B. Webb, and D. F. Williams, Phys. Rev. B **25**, 7836 (1982).
[16] A. Sarkar, S. Ghosh, S. Chaudhuri, and A. K. Pal, Thin Solid Films **204**, 255 (1991).
[17] S. Brehme, F. Fenske, W. Fuhs, E. Nebauer, M. Poschenrieder, B. Selle, and I. Sieber, Thin Solid Films **342**, 167 (1999).
[18] A. V. Singh, R. M. Mehra, A. Yoshida, and A. Wakahara, J. Appl. Phys. **95**, 3640 (2004).
[19] H. K. Muller, Phys. Status Solidi **27**, 733 (1968).
[20] H. Kostlin, R. Jost, and W. Lems, Phys. Status Solidi A **29**, 87 (1975).
[21] R. Clanget, Appl. Phys. **2**, 247 (1973).
[22] Y. Ohhata, F. Shinoki, and S. Yoshida, Thin Solid Films **59**, 255 (1979).
[23] T. Nagatomo, Y. Maruta, and O. Omoto, Thin Solid Films **192**, 17 (1990).
[24] M. Chen, Z. L. Pei, X. Wang, Y. H. Yu, X. H. Liu, C. Sun, and L. S. Wen, J. Phys. D **33**, 2538 (2000).
[25] D. L. Young, T. J. Coutts, V. I. Kaydanov, A. S. Gilmore, and W. P. Mulligan, J. Vac. Sci. Technol. A **18**, 2978 (2000).
[26] J. A. Woollam, W. A. McGahan, and B. Johs, Thin Solid Films **241**, 44 (1994).
[27] T. Gerfin and M. Gratzel, J. Appl. Phys. **79**, 1722 (1996).
[28] R. A. Synowicki, Thin Solid Films **313–314**, 394 (1998).
[29] J. A. Dobrowolski, L. Li, and J. N. Hilfiker, Appl. Opt. **38**, 4891 (1999).
[30] K. Zhang, A. R. Forouhi, and I. Bloomer, J. Vac. Sci. Technol. A **17**, 1843 (1999).
[31] L. Meng, E. Crossan, A. Voronov, and F. Placido, Thin Solid Films **422**, 80 (2002).
[32] H. El Rhaleb, E. Benamar, M. Rami, J. P. Roger, A. Hakam, and A. Ennaoui, Appl. Surf. Sci. **201**, 138 (2002).
[33] M. Losurdo, Thin Solid Films **455–456**, 301 (2004).
[34] G. J. Exarhos, A. Rose, and C. F. Windisch, Jr., Thin Solid Films **308–309**, 56 (1997).
[35] K. Postava, H. Sueki, M. Aoyama, T. Yamaguchi, K. Murakami, and Y. Igasaki, Appl. Surf. Sci. **175–176**, 543 (2001).
[36] H. Fujiwara, M. Kondo, and A. Matsuda, J. Appl. Phys. **93**, 2400 (2003).
[37] M. Miyazaki, K. Sato, A. Mitsui, and H. Nishimura, J. Non-Cryst. Solids **218**, 323 (1997).
[38] K. Ellmer, J. Phys. D **34**, 3097 (2001).
[39] T. Minami, H. Sato, K. Ohashi, T. Tomofuji, and S. Takata, J. Cryst. Growth **117**, 370 (1992).
[40] T. Pisarkiewicz, K. Zakrzewska, and E. Leja, Thin Solid Films **174**, 217 (1989).
[41] D. H. Zhang and H. L. Ma, Appl. Phys. A: Mater. Sci. Process. **64**, 487 (1996).
[42] K. Peter, G. Willeke, K. Prasad, A. Shah, and E. Bucher, Philos. Mag. B **69**, 197 (1994).
[43] T. Sameshima, K. Saitoh, M. Sato, A. Tajima, and N. Takashima, Jpn. J. Appl. Phys., Part 2 **36**, L1360 (1997).
[44] H. Fujiwara, M. Kondo, and A. Matsuda, Appl. Phys. Lett. **83**, 4348 (2003).
[45] T. E. Tiwald, D. W. Thompson, J. A. Woollam, W. Paulson, and R. Hance, Thin Solid Films **313–314**, 661 (1998).
[46] R. M. A. Azzam and N. M. Bashara, *Ellipsometry and Polarized Light* (North-Holland, Amsterdam, 1987).
[47] J. Lee, P. I. Rovira, I. An, and R. W. Collins, Rev. Sci. Instrum. **69**, 1800 (1998).
[48] Y. H. Yang and J. R. Abelson, J. Vac. Sci. Technol. A **13**, 1145 (1995).
[49] K. Forcht, A. Gombert, R. Joerger, and M. Kohl, Thin Solid Films **302**, 43 (1997).
[50] M. Kildemo, R. Ossikovski, and M. Stchakovsky, Thin Solid Films **313–314**, 108 (1998).
[51] C. M. Herzinger, B. Johs, W. A. McGahan, J. A. Woollam, and W. Paulson, J. Appl. Phys. **83**, 3323 (1998).
[52] D. E. Aspnes, Thin Solid Films **89**, 249 (1982).
[53] H. Fujiwara, J. Koh, P. I. Rovira, and R. W. Collins, Phys. Rev. B **61**, 10 832 (2000).
[54] P. I. Rovira and R. W. Collins, J. Appl. Phys. **85**, 2015 (1999).
[55] G. E. Jellison, Jr. and F. A. Modine, Appl. Phys. Lett. **69**, 371 (1996); **69**, 2137(E) (1996).
[56] E. Shanthi, V. Dutta, A. Banerjee, and K. L. Chopra, J. Appl. Phys. **51**, 6243 (1980).
[57] E. Shanthi, A. Banerjee, V. Dutta, and K. L. Chopra, J. Appl. Phys. **53**, 1615 (1982).
[58] D. E. Aspnes, A. A. Studna, and E. Kinsbron, Phys. Rev. B **29**, 768 (1984).
[59] H. Yoshikawa and S. Adachi, Jpn. J. Appl. Phys., Part 1 **36**, 6237 (1997).
[60] G. E. Jellison, Jr. and L. A. Boatner, Phys. Rev. B **58**, 3586 (1998); **65**, 049902(E) (2001).
[61] A. B. Djurisic, Y. Chan, and E. H. Li, Appl. Phys. A: Mater. Sci. Process. **76**, 37 (2003).
[62] F. Wooten, *Optical Properties of Solids* (Academic, New York, 1972).
[63] R. W. Collins and K. Vedam, in *Encyclopedia of Applied Physics*, edited by G. L. Trigg (VCH, New York, 1995), Vol. 12, p. 285.
[64] C. Tanguy, Phys. Rev. B **60**, 10 660 (1999).